Photoionization of neon between 100 and 2000 eV: Single and multiple processes, angular distributions, and subshell cross sections*

F. Wuilleumier† and M. O. Krause
Transuranium Research Laboratory, Oak Ridge National Laboratory, Oak Ridge, Tennessee 37830
(Received 20 March 1974)

All aspects of photoionization in the soft-x-ray region are taken into account, and a complete partitioning of the photoionization cross section of neon is given in terms of single-electron processes in $2p$, $2s$, and $1s$ subshells and multiple-electron processes involving these subshells. The various processes, including their angular dependences, are identified and studied by the technique of photoelectron spectrometry. The partition relies solely on experimental evidence. Absolute subshell cross sections for the emission of a single electron are compared with current theoretical predictions: The single-particle, frozen-structure model (Cooper, 1962) that uses the Herman-Skillman potential overestimated σ_{2p} by up to 15%, σ_{2s} by (25–35)%, and σ_{1s} by about 20%; the random-phase-approximation-with-exchange model (Amusia, 1972) that includes multielectron correlation and uses Hartree-Fock wave functions predictions correctly σ_{2s} at $110 < h\nu < 220$ eV, where comparative data exist. The absolute cross section for double ionization in the L shell is 5×10^{-20} cm^2 at $h\nu = 278$ eV as compared with the theoretical value of 4×10^{-20} cm^2. The energy dependence of simultaneous excitation and ionization processes in the L shell is reported. A finite threshold value is observed and a plateau at higher energy is indicated. For $h\nu > 130$ eV, $\epsilon l, n'l'$ transitions are found to be most probable in which the continuum electron changes its angular momentum, $\Delta l = \pm 1$, and the excited electron retains its momentum, $\Delta l = 0$, namely $2p^6 \rightarrow 2p^4 \epsilon d, np$. Anisotropy parameters β for $2p$ electrons agree well with theoretical results; however an unexplained maximum near $\theta = 0°$ at $h\nu > 1$ keV is found for the angular distributions of $2p$ photoelectrons.

I. INTRODUCTION

A complete partition of the photoionization cross section into its partial cross sections, with differentiation according to single and multiple processes, is much needed if we are to deepen our understanding of the photon-atom interaction and improve the reliability of total and partial cross-section values. Experimental data are especially needed in the ultrasoft-x-ray range, $h\nu \lesssim 1$ keV, where the photon interacts with electrons in the outer region of the atom, and electron-electron correlation of different types may play an important role. Furthermore, accurate subshell cross sections are essential to quantitative chemical analysis by photoelectron spectrometry, and fluorescence x-ray and Auger-electron spectrometry. To the present time a partition of the photoionization cross section into all its components has not been realized.

In this study, we used the technique of photoelectron spectrometry to delineate the various aspects of the photoionization process, and to give a quantitative account of photoionization of neon between 100 and 2000 eV. Specifically, we determined the following quantities as a function of photon energy: (a) relative differential photoionization cross sections for the ejection of a single electron from $1s$, $2s$, and $2p$ subshells at $\theta = 90°$ and $\theta = 54.73°$ between the photon and photoelectron propagation vectors; (b) relative probabilities of $\epsilon l, n'l'$ processes, often referred to as shakeup processes, in which an L electron is excited to the $n'l'$ state concomitant with the ionization of another L electron into an ϵl channel; (c) energies of photoelectrons arising from $\epsilon l, n'l'$ processes involving $2p$ electrons; (d) angular distributions of $2p$ photoelectrons, or alternatively, the anisotropy parameter β_{2p}; and (e) angular dependence of $\epsilon l, n'l'$ processes involving $2p$ electrons.

Using these data and earlier data on double-ionization, $\epsilon l, \epsilon' l'$ processes, and on $\epsilon l, n'l'$ transitions involving the $1s$ shell, we were able to partition the total photoionization cross section σ_{tot}, which is known to a great degree of accuracy, into its components and thereby obtain *absolute* partial cross sections σ_{nl} for *single*-electron transitions and *absolute* cross sections $\sigma_{\epsilon l, \epsilon' l'}$ and $\sigma_{\epsilon l, n'l'}$ for *multiple*-electron transitions. Data of this sort, obtained for the first time over an extended range of energies, allowed us to apply a stringent and detailed test of current theoretical models in the nonrelativistic region. In addition, the angular distributions and energies of photoelectrons emitted in $\epsilon l, n'l'$ processes yielded further insight into the nature of the multiple-electron transitions.

Only few measurements going beyond the determination of the total photoionization cross section have been carried out in the past, and most of these studies had limited objectives. For exam-

ple, Krause[1] measured relative differential cross sections for M and N subshells of Kr in the soft-x-ray region; Samson and Cairns[2] measured subshell cross-section ratios for the outermost shells of the rare gases at very low energies, $h\nu \lesssim 30$ eV; Siegbahn *et al.*[3] determined differential cross section ratios for $2p$ and $2s$ electrons of elements $4 \leq Z \leq 23$ at several isolated photon energies; Lynch *et al.*[4] measured the $\sigma_{3p}(\hat{k})/\sigma_{3s}(\hat{k})$ ratio for argon at $h\nu \lesssim 30$ eV; and a number of investigators studied $\epsilon l, n'l'$ processes for KL and LL shells of neon[3,5-8] and a number of other shells of the other rare gases.[9,10] While the above investigations used the technique of photoelectron spectrometry, other techniques were employed to obtain relative intensities of $\epsilon l, \epsilon' l'$ processes for KL and LL electrons of neon.[6,9,11-13] Finally, anisotropy parameters β were determined for p electrons of the outer shells of the rare gases[14-17] at energies below 50 eV, for $3p$ and $3d$ electrons of krypton and $1s$ electrons of neon between 300 and 1500 eV,[1] and for $\epsilon l, n'l'$ transitions in helium[18] semi-empirically between 100 and 200 eV.

We reported previously[19] preliminary results of some aspects of this study, and we presented elsewhere[20] values of the anisotropy parameter, and differential and partial cross sections for all subshells between 50 and 3000 eV in tabular and graphic form for those workers who may need this type of data for reference purposes in a number of applications as, e.g., energy-dispersive x-ray analysis by means of photoelectron spectrometry.[21] In this paper we give a full account of the work.

II. EXPERIMENTAL

As in previous studies[11,18-22] in which we utilized the technique of electron spectrometry, we employed a double-focussing electrostatic energy analyzer and a number of different x-ray anodes and source chambers. Since we have not given a detailed description of the experimental setup before, we take this opportunity to present the essential features of the apparatus, operating mode, and procedures.

A. Apparatus

In Fig. 1 the analyzer and one of the source-chamber configurations used, the rotatable chamber, are shown. The spherical sector plates, machined of aluminum, enclose angles of 140° and 60° and define a mean radius of 152 mm within a 28-mm gap having a tolerance of 10 μm. The plates are enclosed in an aluminum housing which is evacuated by an oil diffusion pump to a base pressure of 3×10^{-5} N/m^2 (133.3 N/m^2 = 1 Torr). The detector chamber contains normally a Mullard continuous electron multiplier with the entrance funnel biased near ground potential.

In contrast to an earlier version,[1] which is now being used[14] with a helium discharge tube, the present rotatable chamber allows for a coplanar arrangement of x-ray tube and median plane of the analyzer, thus giving continuous coverage of the angular range $-85° \leq \theta \leq 120°$ ($-100° \leq \theta \leq 140°$, if needed). All surfaces seen by the electrons before entering the analyzer are uniformly covered by carbon black. A fixed-source chamber, depicted elsewhere,[21] is designed for work in the gas phase and provides ports for an x-ray tube, electron gun, and discharge tube, each located at right angles with the electron optical axis. The x-ray tube, transferable between fixed and rotatable chamber, was designed for ready exchange of anodes and windows and generates photons over a wide range of energies, namely $100 \lesssim h\nu \lesssim 5000$ eV. The tube is pumped separately and operated at a pressure below 1×10^{-4} N/m^2. The entire system is enclosed in a double high-permeability magnetic shield, which reduces ambient magnetic fields to about 3 mOe along the electron path.

Although electron optical aberrations are at minimum for $\phi = 180°$,[23] no serious deterioration of resolution occurs for $\phi = 140°$ as used here. A resolution of $\Delta E/E = 5\times10^{-4}$ can be achieved,[11] but for the sake of higher intensity $\Delta E/E = 0.15\%$ is commonly used. Entrance and exit slits are typically 7×0.2 mm for the fixed chamber and 4×1 mm for the rotatable one. With identical entrance- and exit-slit dimensions the trans-

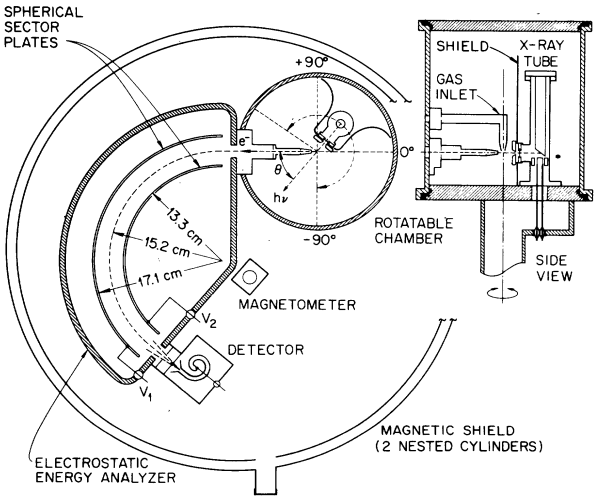

FIG. 1. Schematic of 15-cm electrostatic double-focussing electron energy analyzer. Rotatable chamber can be replaced by fixed chamber for work with gaseous or solid samples and the use of x rays, electrons, or photons from discharge tube as excitation sources.

mission function is substantially Gaussian and the transmitted flux is proportional to the energy of the electrons.[24]

B. Mode of operation

Electrons are counted individually and normally are not subjected to pre- or postacceleration, although this option can be applied. Data acquisition is automatic and follows the procedure developed earlier for the original 90° instrument.[25] A preset energy range, variable from 2 to 500 eV, is swept repetitively by applying a dc biased positive sawtooth potential to the inner plate and a negative sawtooth of the same magnitude to the outer plate, and by storing the detector signal in the memory of a multichannel scaler whose channel advance is synchronized with the sawtooth waveform. Since the plate potentials are proportional to the kinetic energy of the focussed electron, each channel corresponds to a definite electron energy. In practice, a master pulse triggers simultaneously the multiscaler and the oscilloscope that provides the sweep every 50 msec; and the sawtooth, $\tau = 46$ msec, taken from the cathode-ray tube is superimposed on a precision voltage bias, variable from 0 to 3 kV. Although sawtooth and channel advance are synchronized only at the start of each scan, their respective stabilities are sufficiently good even for the duration of several days to render a data display that is stable within 1 channel. The linearity of the energy scale is about 1/500 of the range that is determined by the sawtooth. The particular advantage of this system of data handling lies in the automatic averaging procedure, since a given energy interval is scanned at least 10^4 times, thus placing no further demands on the stability of incident x-ray flux and sample density beyond those mild demands set by the need to keep changes of the space charge (and surface charges) in the sample chamber within certain limits.

Scale linearity and calibration in terms of eV per channel are checked and determined by means of electrons from a thermionic source with precisely known accelerating voltages. The same electron source also allows the determination of the conversion factor $f = dE/dV$ between electron energy E and plate potential V, $f = 4.0465(15)$, and yields a rough absolute-energy calibration. However, an accurate absolute calibration of the energy scale is based on suitable Auger or photoelectron reference lines and requires the inclusion of a relativistic correction in the factor f.

C. Operating procedure and conditions

In this experiment, high-resolution data, $\Delta E/E = 0.15(1)\%$, were taken at $\theta = 90°$ in the scanning mode described above using the fixed source chamber. With sample pressures ranging from 5 to 10 N/m^2 (absolute) in the source and from 1 to 3 mN/m^2 in the analyzer (ionization gauge reading), runs required between 1 and 20 h to accumulate more than 10^4 counts in the main peak. Measurements of angular distributions and those at the angle $\theta = \theta_0 = 54.73°$ were made with $\Delta E/E = 1\%$ using the rotatable chamber, Fig. 1. In this instance, the sample pressure was reduced to about 2 N/m^2 to minimize effects from electron-atom scattering processes and to prevent a gaseous discharge between chamber walls and the x-ray tube anode which was elevated to high voltage. When angular distributions were measured, analyzer-plate voltages were set to pass only electrons of the desired energy, and the angular adjustments were made manually. At each setting of θ, counting continued until a statistical confidence of better than 5% was achieved, which required between 30 and 200 sec for the various photon sources. Short term fluctuations of x-ray flux and sample gas pressure were generally within the counting statistics, and long term drifts of the x-ray line intensity were checked and compensated for by periodically referring the count rates to measurements at the reference angle $\theta = 90°$. Angular resolution was $4.7 \pm 0.7°$, where the "error limits" refer to the half-shadow fringes. Proper operation of the chamber was tested by recording known angular distributions of several photo- and Auger-electron lines, such as He $1s(\mathrm{Zr}M\zeta)$, Ne $2s(\mathrm{Y}M\zeta)$, Ne $2s(\mathrm{Zr}M\zeta)$, Ne $1s(\mathrm{Mg}K\alpha)$, and Ne $1s - 2p2p(^1D_2)$. Except for reduction to equal source volume,[26] no other correction needed to be applied at any energy or angle but for $\theta = 5°$, where part of the x-ray beam struck the edges of the entrance aperture. This correction was large and difficult to assess precisely so that data at $\theta = 5°$ are somewhat uncertain.

Although we shall discuss correction to the data and their uncertainties in Sec. IV as required, we point out here that we considered the following variables: x-ray flux, gas pressure, plate voltages, electron transmission, detector response, elastic and inelastic scattering, background from various sources, interfering and overlapping peaks, effective source volume, and space charge.

A variety of elements supplied characteristic x rays whose energies ranged from 108.9 eV for Be K to 2042 eV for Zr $L\alpha$, and whose natural widths varied from 0.47 eV for Y $M\zeta$ and 0.65 eV for Mg $K\alpha$ to about 5 eV for Be K and O K from Al_2O_3. X rays up to $h\nu = 1$ keV were transmitted through a 0.2-μm polystyrene foil (in one case carbon foil), and x rays above $h\nu = 1$ keV through a 12.5-μm beryllium foil. While either type of

window provided a complete separation of the vacua of gas cell and x-ray tube, the polystyrene foils were not opaque to high-energy electrons and required the anode to be operated at positive potential and the cathode at or near ground to prevent electrons from entering the gas cell and, in fact, to avoid untimely destruction of the foil by electron bombardment. We note that for anodes supplying x rays of $h\nu \gtrsim 500$ eV a takeoff angle of 7° to 10° was used, and for those generating x rays of $h\nu \lesssim 500$ eV an angle of 20° to 25° was used with the latter resulting in a twofold to threefold intensity increase over the intensities previously reported for an angle of 7°.[25]

III. BASIC RELATIONS

We present in this section the basic relations and procedures that underlie this investigation. In the dipole approximation and for random orientation of the target, the differential photoionization cross section for a subshell nl is given by

$$\sigma_{nl}(\hat{k}) = \frac{\sigma_{nl}}{4\pi}\left[1+\beta_{nl}\left(\frac{3\cos^2\phi - 1}{2}\right)\right] \tag{1}$$

for polarized radiation, and by

$$\sigma_{nl}(\hat{k}) = \frac{\sigma_{nl}}{4\pi}\left[1-\frac{\beta_{nl}}{2}\left(\frac{3\cos^2\theta - 1}{2}\right)\right] \tag{2}$$

for unpolarized radiation.

The angle ϕ is the angle between polarization direction and photoelectron propagation vector, and θ is the angle between x-ray and photoelectron propagation directions. The angular anisotropy parameter $\beta_{nl} = \beta(R_{l\pm1}, l, \delta)$ is a function of the matrix elements $R_{l\pm1}$, the angular momentum quantum number l, and the phase shift δ. It assumes the values $-1 \leq \beta_{nl} \leq 2$ in the general case and is 2 for s electrons.[27]

Assuming unpolarized radiation in the following, the partial or subshell cross section σ_{nl} can be obtained experimentally by measuring $\sigma_{nl}(\hat{k})$ at an arbitrary angle θ and also β_{nl} or, alternatively, by measuring $\sigma_{nl}(\hat{k})$ at the so-called magic angle $\theta_0 = 54.73°$, since then

$$\sigma_{nl}(\hat{k}) = \sigma_{nl}/4\pi \tag{3}$$

independent of β_{nl}. This latter procedure presupposes the validity of relation (2) or its often used equivalent form

$$\sigma_{nl}(\hat{k}) = A + B\sin^2\theta, \tag{4}$$

with $A + B = 100$ and $\beta_{nl} = 4B/(3A+2B)$. If, however, retardation can no longer be neglected, as for $h\nu \gtrsim 2$ keV, one measurement at θ_0 is insufficient since angular distributions become skewed in the forward direction. Equation (2) or (4) is replaced by more complex expressions, such as the often used, though approximate relation[28]

$$\sigma_{nl}(\hat{k}) = A + B\{1 + [(4+l)v/c]\cos\theta\}\sin^2\theta, \tag{5}$$

where l is the orbital quantum number and v/c the relative photoelectron velocity.

The total photoionization cross section, which is extracted from absorption measurements following correction for photon scattering or obtained directly from ion-chamber measurements, contains all individual cross sections for single-, double-, triple-photoionization processes in the subshells nl:

$$\sigma_{\rm tot} = \sum_{nl}\sigma_{nl} + \sum_{nl,n'l'}\sigma_{nl,n'l'} + \text{triple} + \cdots, \tag{6}$$

where $\sigma_{nl,n'l'}$ designates the cross section for double-electron transitions from nl and $n'l'$ shells. Similarly, the cross section that is obtained theoretically is composed of the subshell contributions σ'_{nl} (which are calculated):

$$\sigma_{\rm tot} = \sum_{nl}\sigma'_{nl}. \tag{7}$$

We distinguish the subshell cross section in Eq. (7) from that in Eq. (6) by a prime since it is not self-evident that they are identical. In fact, it has not been examined in the past whether σ'_{nl} contains only single-electron processes or whether it contains also multiple-electron processes. Only very recently has it been shown[29] that theoretical calculations based on the commonly employed frozen-structure approximation lead to subshell cross sections σ'_{nl} that include multiple processes associated with the level nl. Consequently, calculations of this type do not provide a detailed breakdown of $\sigma_{\rm tot}$ as indicated by Eq. (6). On the other hand, more sophisticated calculations[30-32] are capable of distinguishing between the single- and multiple-photoionization processes.

Experimentally, photoelectron spectrometry can distinguish the various single and multiple processes by the kinetic energy the photoelectron acquires. We have

$$E_{e,\rm kin}(\epsilon l) = h\nu - E_{nl} \tag{8}$$

for the photoemission of a single electron from the nl level;

$$E_{e,\rm kin}(\epsilon l, n'l') = h\nu - E_{nl} - E_{n''l''\to n'l'} \tag{9}$$

for the simultaneous emission of an electron from the nl level and the excitation of another electron from the $n''l''$ level to some $n'l'$ level, an $\epsilon l, n'l'$ process; and

$$E_{e,\rm kin}(\epsilon l, \epsilon' l') = h\nu - E_{nl} - E_{n''l''} - E^*_{e,\rm kin}(\epsilon' l', \epsilon l) \tag{10}$$

for the simultaneous ejection of two electrons from nl and $n''l''$ levels, an $\epsilon l, \epsilon' l'$ process. Evidently, discrete lines are associated with ϵl and $\epsilon l, n'l'$ processes, Eqs. (8) and (9), provided $h\nu$ is discrete, and a continuum consisting of two indistinguishable parts is associated with $\epsilon l, \epsilon' l'$ processes, Eq. (10).

Intensities of photoelectron lines or continua are proportional to the differential cross section of the process selected energetically, namely,[20,21]

$$I_x(e) = C\eta(1-\alpha)E_x(e)T(h\nu)I(h\nu)\sigma_x(\hat{k}), \tag{11}$$

where x stands for nl; $nl, n'l'$; etc. C is a constant, $\eta = \eta(E)$ the detector efficiency, $\alpha = \alpha(E)$ the fraction of electrons scattered out of the beam, $E_x(e)$ the photoelectron energy, $T = T(h\nu)$ the x-ray window transmission, and $I(h\nu)$ the intensity of the unpolarized x rays. This relation holds for an electrostatic analyzer with identical entrance and exit apertures, with no preacceleration and a sufficiently small acceptance angle. According to Eq. (11), $\sigma_x(\hat{k})$ can be determined absolutely if all the other quantities are known, including the constant C, which contains the density and volume of the converter gas and the various solid angles. However, in many instances it suffices to determine $\sigma_x(\hat{k})$ on a relative scale, so that only the energy dependence of the parameters in Eq. (11) need be known.

In this study, we determined relative differential cross sections $\sigma_x(\hat{k})$ according to Eq. (11) for all processes,[33] converted these into relative cross sections σ_x, using either β_x or Eq. (3), and normalized the σ_x to the total photoionization cross section σ_{tot} known from the literature. Thus the cross sections σ_x and $\sigma_x(\hat{k})$ are obtained on an absolute scale, Schematically,

$$\sigma_{x,\text{rel}}(\hat{k}) \xrightarrow{\beta_x} \sigma_{x,\text{rel}} \xrightarrow{\sigma_{\text{tot}}} \sigma_{x,\text{abs}} \xrightarrow{\beta_x} \sigma_{x,\text{abs}}(\hat{k}). \tag{12}$$

Since customarily many observations are carried out at $\theta = 90°$, we like to express the ratio σ_{2s}/σ_{2p} in terms of the differential cross sections at 90° or at θ_0:

$$\frac{\sigma_{2s}}{\sigma_{2p}} = \frac{\sigma_{2s}(\hat{k})}{\sigma_{2p}(\hat{k})}\bigg|_{\theta_0} = \frac{2(1+\beta_{2p}/4)}{3}\,\frac{\sigma_{2s}(\hat{k})}{\sigma_{2p}(\hat{k})}\bigg|_{90°}. \tag{13}$$

According to many-electron selection rules[34] there may be an excitation of two electron states (a) if one electron changes only its n and the other electron changes n by an arbitrary amount *and* its l by ± 1, or (b) if both electrons change their n's by arbitrary amounts and one its l by γ and the other its l by $\delta \pm 1$, with the condition $\gamma + \delta =$ even. Photoabsorption measurements have shown[35] that case (a) yields the most intense $nl, n'l'$ transitions for double excitation of $2p$ electrons of neon.

Analogously, we expect the $\epsilon l, n'l'$ transitions $2p^6 \rightarrow 2p^4\epsilon d, 3p$ (or $\epsilon s, 3p$), $2p^6 \rightarrow 2p^4\epsilon p, 3s$, and $2p^6 \rightarrow 2p^4\epsilon p, 3d$ to be predominant. As we have pointed out earlier in the case of helium,[18] it is of interest to separate the different transitions to be able to determine whether the continuum electron changes its l, viz., $\epsilon d, 3p$ ($\epsilon s, 3p$), or the excited electron changes its l, viz., $\epsilon p, ns$ or $\epsilon p, nd$. Separation can be accomplished on the basis of energy and/or angular distribution measurements. From symmetry considerations[36] we might expect that the angular distributions of the transitions

$$2p^6 \rightarrow 2p^4\epsilon d, 2p, \tag{14a}$$

$$2p^6 \rightarrow 2p^4\epsilon d, 3p \tag{14b}$$

are characterized by the same anisotropy parameter β_p [the weak $\epsilon s, np$ channel is omitted in Eq. (14)]. Similarly, the transitions

$$2s^2 2p^6 \rightarrow 2p^6\epsilon p, 2s, \tag{15a}$$

$$2s^2 2p^6 \rightarrow 2s^2 2p^4\epsilon p, 3s \tag{15b}$$

would have the parameter β_s, $\beta_s \neq \beta_p$; and

$$2p^6 \rightarrow 2p^4\epsilon p, 3d \tag{16}$$

a parameter β_d which in general would be different from β_p and certainly different from $\beta_s = 2$.

Thus the final configurations of the double transitions, Eqs. (14b), (15b), and (16), which satisfy the dipole selection rules, can be recognized and distinguished by an angular measurement: Transition (14b) would have the same β_p value as the single-electron transition (14a) ($2p$ photoline); and transition (15b) would have the same β_s as the single-electron transition (15a) ($2s$ photoline). Though it is, in principle possible that $\beta_s \approx \beta_p \approx \beta_d$ at a certain photon energy $h\nu$, this situation is unlikely to occur[37] and can be avoided by using different excitation energies.

IV. RESULTS AND DISCUSSION

A. Photoelectron spectrum

Typical photoelectron spectra recorded at $\theta = 90°$ and $\Delta E/E = 0.15\%$ are shown in Fig. 2. In accordance with Eqs. (8) and (9), the $2p$ and $2s$ photolines signify the emission of a single, and only a single, electron from the $2p$ and $2s$ subshells, respectively; peaks j, i, and h signify the ejection of a $2p$ electron and the simultaneous excitation of a $2p$ electron into a discrete, bound level, an $\epsilon l, n'l'$ process; and peaks o and n signify $\epsilon l, n'l'$ processes involving a $2s, 2p$ electron pair. The peaks c indicate energy losses suffered by a $2p$ or $2s$ photoelectron in collisions with neutral neon atoms. Although corrections necessary to

convert these raw data into cross sections have not been applied, the spectra show the essential features of photoionization in the L shell of neon, that is, the predominance of σ_{2p} at low photon energies, the increasing importance of σ_{2s} at higher energies, and the small but not unimportant cross section for multiple processes.

An enlarged view of the region in which $\epsilon l, n'l'$ processes involving the $2p$ electrons occur is shown in Fig. 3. This spectrum was recorded with particular care to achieve the best possible resolution that can be gotten without monochromatization of the x rays. Note the great number of peaks that have emerged. As indicated in the figure, most peaks can be correlated with energy levels known from optical spectroscopy.[38] The spectrum of Fig. 3 was generated by Y $M\zeta$ x rays, but similar spectra, though less well resolved, were obtained with Zr $M\zeta$ and Nb $M\zeta$ x rays.

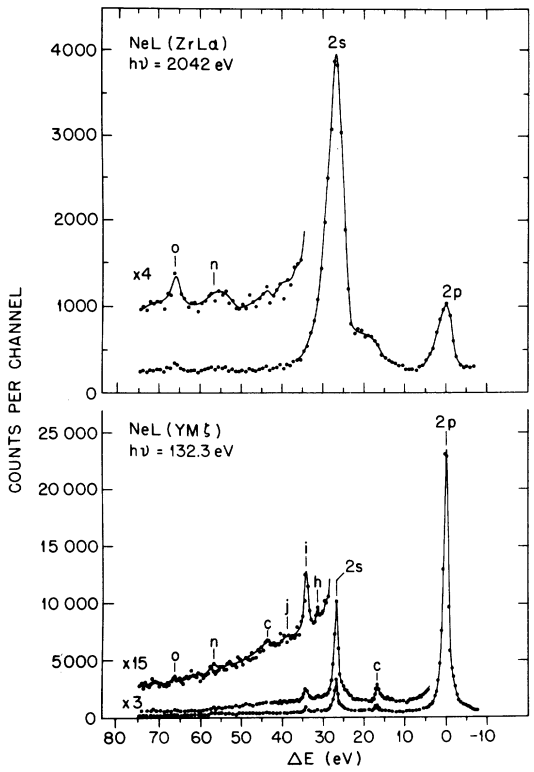

FIG. 2. Typical photoelectron spectra as recorded. Peaks, labeled $2s$ and $2p$, are due to the ejection of a single electron from $2s$ and $2p$ subshells; peaks, labeled n, o, j, i, h, are due to the simultaneous ejection of an L electron and excitation of another L electron; peaks c indicate characteristic energy losses. Spectra were recorded automatically at $\theta = 90°$ and $\Delta E/E = 0.15\%$; peak heights are representative of relative differential and, to a lesser degree, integrated subshell cross sections.

B. Differential cross-section ratios for $\sigma_{2s}(\hat{k})/\sigma_{2p}(\hat{k})$ at 90° and θ_0

From spectra such as those shown in Fig. 2 we deduced the differential cross-section ratios $\sigma_{2s}(\hat{k})/\sigma_{2p}(\hat{k})$ at $\theta = 90°$ in the energy range $109 \leq h\nu \leq 2042$ eV. They are listed in Table I together with pertinent characteristics of the x-ray lines. These ratios as well as those given in the following tables are obtained from the photopeak-area values following correction for background, for interfering lines as in the case of Ne $2s$ (Cu $L\alpha$), and following conversion into differential cross-section ratios by means of Eq. (11). The factor $E(e)$ in Eq. (11) is automatically obtained, $\eta = \eta(E)$ was measured in an auxiliary experiment by postaccelerating electrons, α did not exceed 0.03 under our experimental conditions, and the ratio $(1 - \alpha_{2s})/(1 - \alpha_{2p})$ varied less than 0.3% for the interval of 28 eV between the $2s$ and $2p$ photolines. The correction for electron scattering was therefore omitted, a step which was additionally justified by an auxiliary experiment in which the ratios were found to be identical within the error bounds of 0.5%, although the source pressure differed widely, 0.1 and 1.5 N/m^2, and although the photons, Zr $M\zeta$ (151.4 eV), produced electrons in a region of rapidly varying scattering cross sections. Quoted errors take into account counting statistics, number of runs (typically three), and uncertainties in the corrections, with the background generally contributing the major part. It is worthwhile to note that peak values gave identical though inherently less accurate results. Similarly, ratios determined with the rotatable-chamber arrangement, $\Delta E/E = 1\%$, agreed excellently with the high-resolution data despite different solid angles, different source pressures and different pressure gradients in the slit systems. Only for Be K (109 eV), a small and presumably accidental difference was noted, and the value in Table I gives the weighted average. The few literature data[3,7] available agree satisfactorily with our results.

Spectra at θ_0 (54.73°) were taken with the x-ray tube placed in the rotatable chamber. No problems arose from potential overlap with other lines at the reduced resolution of 1% nor, as already stated, from the greater solid angle. Differential cross-section ratios, which are presented in Table II, column 2, were analyzed in the same manner as those listed in Table I. Relying on Eq. (13), we calculated the ratios at θ_0 from those at $\theta = 90°$, Table I, using theoretical values[39] of β_{2p}. These ratios are listed in column 4 and compare excellently with the direct measurement, suggesting that theory[39] predicts β_{2p} satisfactorily through

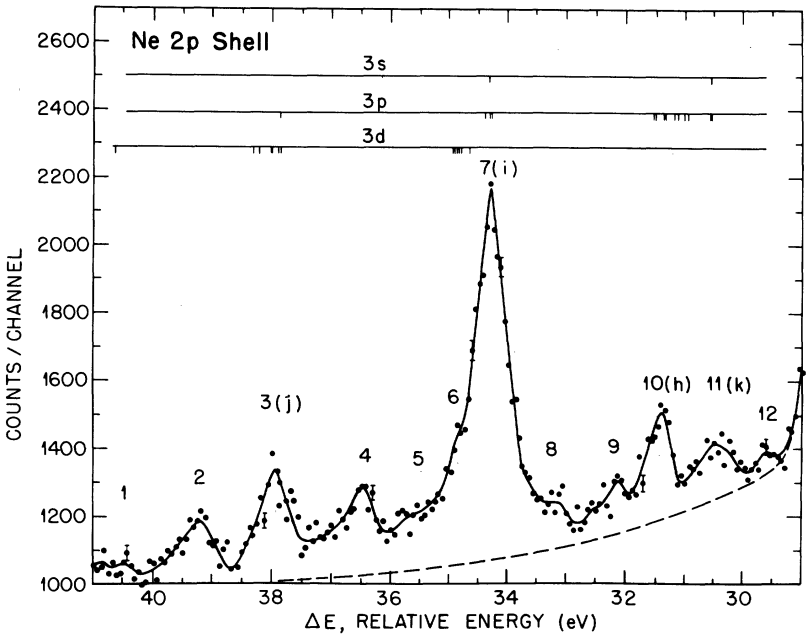

FIG. 3. Spectral scan of region containing $\epsilon l, n'l'$ transitions involving two $2p$ electrons. Scale relative to $E(2p_{3/2}) = 21.565$ eV; $\theta = 90°$, $\Delta E/E = 0.15\%$, and $h\nu = 132.3$ eV (Y $M\zeta$). Letters in brackets are designations previously used (Ref. 7). Dashed line is estimated tail of $2s$ photoline, see Fig. 2. Note that the shoulder 6 has been reproduced in all high-resolution runs. Tick marks give energy positions of Ne^+ ($3s$), ($3p$), or ($3d$) states as reported in Ref. 38.

the entire range of energies.

Again using the experimental ratio at $\theta = 90°$, we calculated the ratio at θ_0 by inserting experimental values of β_{2p} in Eq. (13). The results are displayed in column 3 of Table II and compare excellently with both the directly measured ratio, column 2, and the semitheoretical ratio, column 4. A single discrepancy of 10% exists for C K (278 eV); however, the value at θ_0 was obtained during the "shakedown" of the rotatable chamber several years ago and may therefore contain a certain systematic error.

The experimental differential cross-section ratios are plotted in Fig. 4 and compared with the theoretical ratios calculated by Kennedy and Manson.[39] Experimental and theoretical curves

TABLE I. Differential cross-section ratio $\sigma_{2s}(\hat{k})/\sigma_{2p}(\hat{k})$ at $\theta = 90°$ for neon. Characteristic x-ray lines are identified and natural widths of lines, $\Gamma(h\nu)$, are given as full width at half-maximum.

Line	X rays Energy (eV)	Width (eV)	$\sigma_{2s}(\hat{k})/\sigma_{2p}(\hat{k})$ This work	Previous work
Be K	108.9	5.0	0.135(12)	
Y $M\zeta$	132.3	0.47	0.159(6)	
Zr $M\zeta$	151.4	0.77	0.177(5)	
Nb $M\zeta$	171.4	1.21	0.209(6)	
Mo $M\zeta$	192.3	1.53	0.254(8)	
Ru $M\zeta$	236.9	2.49	0.36(2)	
Rh $M\zeta$	260.1	4.0	0.40(2)	
C K	278	6	0.46(2)	0.39(2)[a]
Ti Ll	395.3	3	0.70(6)	
Ti $L\alpha$	452.2	3	0.78(3)	
O K	524.9	4	0.90(6)	
Cr $L\alpha$	572.8	3	1.04(8)	
Cu $L\alpha$	929.7	3.8	1.72(9)	
Mg $K\alpha$	1253.6	0.65	2.56(9)	2.7[b]
Al $K\alpha$	1486.6	0.85	3.25(15)	3.2[b], 2.73[c]
Zr $L\alpha$	2042	1.7	4.5(3)	

[a] Reference 6.
[b] Scaled from Fig. 4.7 of Ref. 3.
[c] Reference 7.

TABLE II. Differential cross-section ratio $\sigma_{2s}(\hat{k})/\sigma_{2p}(\hat{k})$ at $\theta_0 = 54.73°$ and anisotropy parameter β_{2p}.

Photon energy (eV)	$\sigma_{2s}(\hat{k})/\sigma_{2p}(\hat{k})$ I[a]	II[b]	III[c]	β_{2p} Expt.[d]	Theory[e]
108.9	0.118(7)	0.122(11)	0.123	1.35(2)	1.40
132.3	0.145(5)	0.145(6)	0.146	1.41(2)	1.45
151.4	0.169(6)	0.162(5)	0.161	1.49(3)	1.45
236.9	0.32(2)	[0.33(1)]	0.33	[1.42]	1.42
278	0.36(2)	[0.41(3)]	0.41	[1.40]	1.41
929.7	1.46(9)	[1.43(5)]	1.42	[0.98]	0.87
1253.6	2.1(1)	2.07(8)	2.02	0.85(2)	0.74
1486.6	2.6(2)	2.58(15)	2.52	0.76(2)	0.64

[a] Measured directly at θ_0.
[b] Derived from measured value at $\theta = 90°$ and measured β_{2p} using Eq. (13).
[c] Derived from measured value at $\theta = 90°$ and theoretical β_{2p} (Ref. 39) using Eq. (13).
[d] This work; values in square brackets interpolated presupposing the same trend as given by theory (Ref. 39).
[e] Kennedy and Manson, Ref. 39. For $h\nu < 400$ eV scaled from the curve given in Ref. 39, for $h\nu > 800$ eV kindly communicated to us by S. T. Manson (Ref. 56).

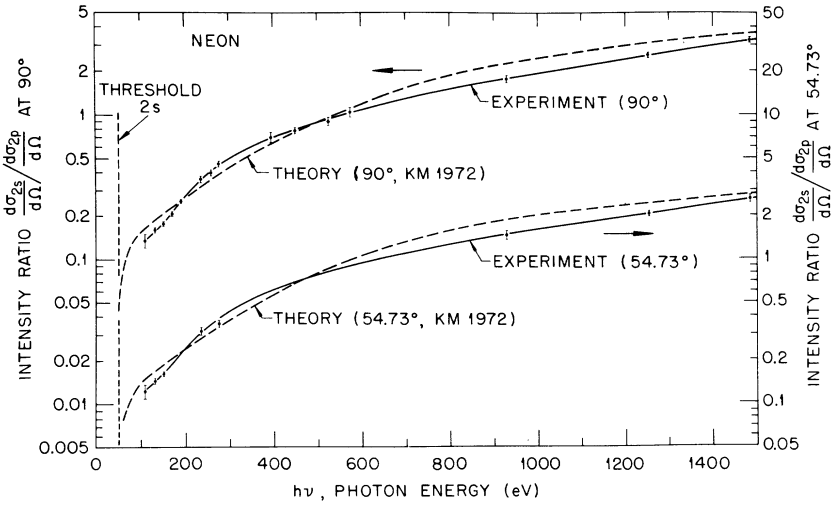

FIG. 4. Differential cross-section ratios for $2s/2p$ subshells of neon, measured at $\theta = 90°$ and at θ_0 (54.73°). Values at θ_0 can be taken to be equivalent to σ_{2s}/σ_{2p}. Theoretical ratios are from Kennedy and Manson (Ref. 39) and Manson (Ref. 56).

exhibit the same general character in the energy range from 100 to 1500 eV, indicating a monotonic increase of the σ_{2s}/σ_{2p} ratio from a value of 0.10 at 100 eV to 2.6 at 1500 eV. To emphasize the discrepancies, we point to the following: (i) Theoretical ratios are higher than experimental ones near threshold and consistently higher at energies above 500 eV; (ii) differences of up to 25% occur; and (iii) the definite undulation in the experimental curves is present but much attenuated in the theoretical curves. The question whether inadequacies in the predictions of the σ_{2s} or σ_{2p} cross section or both are responsible for the discrepancies cannot be decided from the data of Fig. 4, but must be postponed to Sec. IV G, where σ_{2s} and σ_{2p} will be separated.

C. Angular distribution of neon 2p electrons

Angular distributions of photoelectrons from the $2p$ subshell were measured close to 100 eV and somewhat above 1 keV. Several distributions are displayed in Fig. 5. Each data point represents the average of at least two measurements and error bars reflect the statistical uncertainty, largest for the Mg $K\alpha$ and Al $K\alpha$ distributions, and intensity fluctuations, largest for Be K, Y $M\zeta$, and Zr $M\zeta$ distributions. Distributions for low-energy photoelectrons are well reproduced by formula (2), or alternatively Eq. (4), while distributions for energetic photoelectrons follow fairly well the relation (5), which takes into account retardation effects. However, a second maximum in the distribution near $\theta = 0°$ suggests that Eq. (5) is not entirely adequate to describe the photoionization process for $2p$ electrons of neon. Further studies of this effect, which may also occur in other systems, are warranted, although we could not find such a secondary maximum for s electrons of neon at similar photoelectron energies.

In Table II, experimental and theoretical anisotropy parameters β_{2p} are listed, and in Table III

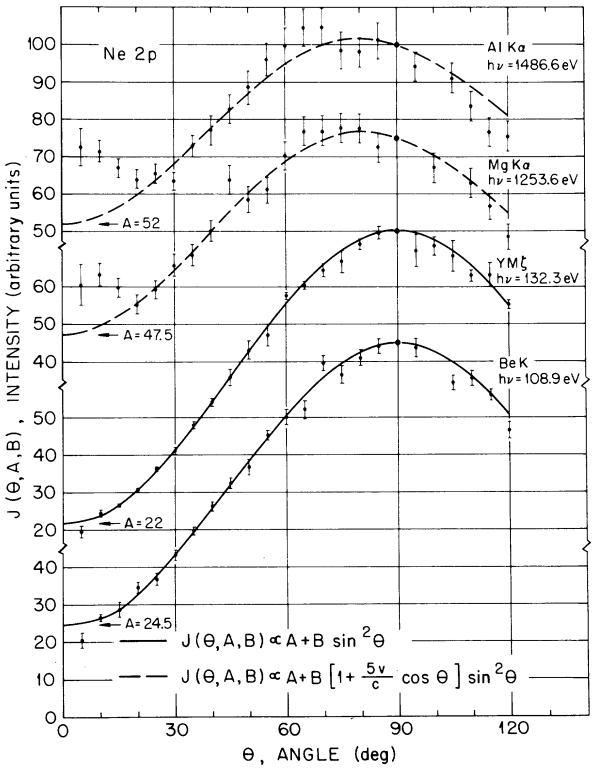

FIG. 5. Angular distributions of Ne $2p$ photoelectrons at low and high energies; $E_e \approx 100$ eV and $E_e \approx 1$ keV. Curves are drawn according to Eqs. (4) and (5) with the parameters A and B fitted; $A + B = 100$. Distributions normalized to 100.0 at $\theta = 90°$.

TABLE III. Parameters A and B of angular distribution of photoelectrons ejected from $2p$ subshell of neon. $A+B=100$.

X-ray line	X-ray energy (eV)	Photoelectron energy (eV)	A	B
Be K	108.9	87.3	24.5(1.0)	75.5(1.0)
Y $M\zeta$	132.3	110.7	22(1)	78(1)
Zr $M\zeta$	151.4	129.8	19(1)	81(1)
Mg $K\alpha$	1253.6	1232.0	47.5(2.0)	52.5(2.0)
Al $K\alpha$	1486.6	1465.0	52(2)	48(2)

the angular distribution parameters are given in terms of A and B [Eqs. (4) and (5)]. We note the isotropic contribution decreases between 100 and 200 eV, as theory predicts,[39] and then increases monotonically toward higher energies, again in accord with theory. In fact, the agreement is excellent in the 100-eV range, which might be compared with a similarly good agreement in the threshold region, $h\nu \lesssim 40$ eV, for the $2p$ electrons of neon,[14-17] and p electrons in the outer shells of the other rare gases.[14,15] Previously[1] we found theory to predict reliably β parameters for $3p$ and $3d$ electrons of Kr and to predict the proper skewing (retardation effect) of the Kr $3s$, $3p$, and $3d$ and the Ne $1s$ distributions.

The agreement with the theoretical β_{2p} is satisfactory at about 1 keV, if we keep in mind that the experimental β_{2p} was derived from Eq. (5), whereas the theoretical β_{2p} was obtained with the neglect of retardation effects. However, neither the skewing nor the secondary maximum introduces any significant error in the ratios σ_{2s}/σ_{2p} and in σ_{nl}, Sec. IV F, since the two effects are small and partially compensatory.

D. Energies, angular distributions, and relative intensities of $\epsilon l, n'l'$ processes in the L shell

The spectral region 28 to 41 eV below the $2p$ photopeak contains lines that are due to $\epsilon l, n'l'$ processes involving two $2p$ electrons and the region between about 50 to 60 eV contains lines that are due to $\epsilon l, n'l'$ processes involving a $2p$ *and* a $2s$ electron. In the hope of identifying the final configurations following these two-electron transitions, we determined the energies of the peaks that are displayed in Fig. 3 with the greatest possible accuracy by using the narrowest characteristic x-ray line available,[22] $\Gamma(\mathrm{Y}\,M\zeta)=0.47$ eV (full width at half-maximum), and other narrow lines such as Zr $M\zeta$ and Nb $M\zeta$. Table IV summarizes the energies relative to Ne $2p_{3/2}$ (21.565 eV), which were averaged from at least five independent determinations per line and 15 determinations for the strongest line $7(i)$. For the weaker lines, errors reflect mainly the difficulty in determining peak positions; for the line $7(i)$, the error reflects mainly a drift of the photoline caused by a decrease of x-ray line intensity with time, which in turn resulted in a decrease of the space charge in the gas cell, corresponding to a change in potential by some 10 meV. In the same table, we list the configurations that can be correlated with the observed peaks on energetic grounds alone and those configurations that are compatible with the required J values[34] of $\frac{3}{2}$ or $\frac{1}{2}$

TABLE IV. Relative energies and intensities of $\epsilon l, n'l'$ transitions (shakeup) involving two $2p$ electrons of neon. Compare with Fig. 3.

Peak No.	Energy (eV)[a] This work[b]	Energy (eV)[a] Table[c]	Intensity[d] (%)	Final states[c]	Assignment[e]
1	40.5–40.7	40.66	2.0	$[2p^4(^1S)3d]\ ^2D$	$3d\ ^2D$
2	39.26(6)	•••	6.9	•••	$2p^4nl;\ n\geq 4$(?)
3(j)	37.97(4)	37.99;37.86	10.7	$[2p^4(^1D)3d]\ ^2P, ^2D, ^2S$;$[2p^4(^1S)3p]\ ^2P^\circ$	$3d\ ^2P, ^2S$;$3p\ ^2P^\circ$
4	36.46(5)	•••	9.8	•••	$2p^4nl;\ n\geq 4$(?)
5	36.1(1)	•••	3.6	•••	$2p^4nl;\ n\geq 4$(?)
6	34.84(6)	34.77–34.93	7.8	$[2p^4(^3P)3d]\ ^4D, ^2D, ^4P, ^2P$	$3d\ ^{2,4}P, ^2D$
7(i)	34.31(3)	34.27;34.29	36.2	$[2p^4(^1D)3p]\ ^2P^\circ, ^2D^\circ$;$[2p^4(^1S)3s]\ ^2S$	$3p\ ^2P^\circ, ^2D^\circ$
8	33.4(1)	33.3	2.9	double-collision peak	•••
9	32.24(6)	•••	4.3	•••	•••
10(h)	31.45(4)	31.52	9.1	$[2p^4(^3P)3p]\ ^2P^\circ, ^2S, ^4S$	$3p\ ^2P^\circ$
11(k)	30.47(5)	30.56	5.4	$[2p^4(^3P)3p]\ ^4P^\circ$;$[2p^4(^1D)3s]\ ^2D$	$3p\ ^4P^\circ$
12	29.62(7)	•••	1.3	•••	•••

[a] Values referred to $E(2p_{3/2})=21.565$ eV.
[b] Values previously obtained (Ref. 7) are $j=38.0$ eV, $i=34.0$ eV, and $(h+k)=30.9$ eV.
[c] Taken from optical-spectroscopy tables of Moore (Ref. 38).
[d] Normalized to total intensity of 100.0%; values refer to spectra obtained at $h\nu=130$–150 eV.
[e] Most probable assignment.

and the results of the angular distribution measurements. Energies of the selected configurations are taken from optical-spectroscopy data,[38] and are given in column 3 of Table IV. It is evident from Fig. 3, where the energies of the final-state configuration are inserted as tick marks, that an experiment at fixed angle θ cannot distinguish between the various states even with the most precise peak-energy determination. Improvements can be made, however, with narrow x-ray lines such as the recently monochromatized Al $K\alpha$ line[8] with $\Gamma_{\text{mono}} = 0.2$ eV at 1.5 keV or low-energy synchrotron radiation yet to be employed.

As demonstrated earlier in the case of helium,[18] angular distribution measurements can resolve such quasidegenerate states as peak $7(i)$, which may be composed of $2p^4(^1D)3p$ and $2p^4(^1S)3s$, to an unknown degree. The experiment we carried out was to measure spectra of the type shown in Fig. 2, at different observation angles θ, namely, at $\theta = 90°$, θ_0, 35° and 20° using Zr $M\zeta$ for excitation and at $\theta = 90$, θ_0, and 30° using Y $M\zeta$. We found in all instances the intensity of peak $7(i)$ to vary in the same way as that of the $2p$ photoline, suggesting that according to Eq. (14) the peak $7(i)$ has by and large p character corresponding to the state $2p^43p$, which is formed by $2p^6 \rightarrow 2p^4\epsilon d, 3p$ (or $\epsilon s, 3p$) transitions. The magnitude of a possible admixture of $2p^43s$ can be estimated from the precision of the measurements: For example, the best run at $\theta = 30°$ yielded for the intensity ratio $I(i)/I(2p)$ relative to the ratio at $\theta = 90°$ a value of 1.03(11), which sets the upper limit of s admixture to 30% of the intensity of the peak $7(i)$, using $\beta_s = 2$ and $\beta_p = 1.41$ in Eq. (2). Taking into account all runs, we arrive at an upper limit of 25%.

Within the precision of the measurements, the line spectrum of Fig. 3 varied with the angle θ like the $2p$ photoline.[40] In addition, no contribution of $2p^43s$ states between $\Delta E = 27.3$ eV and $\Delta E = 27.9$ eV could be discerned on the flank of the $2s$ photoline in the high-resolution spectra, although small contributions such as the one possibly assignable to the peak $7(i)$ could have escaped detection. If we generalize the results of the energy and angular distribution measurements of peaks 6 and 7 to the entire spectrum (cf. Table IV) we can conclude that (i) 18% of all $\epsilon l, n'l'$ transitions involving $2p$ electrons go to a $2p^43d$ state, and (ii) 82% of the transitions go to a $2p^43p$ state with the possibility of up to $\frac{1}{4}$ of these going to a $2p^43s$ state. This result implies that transitions $2p^6 \rightarrow 2p^4\epsilon d, 3p$ (or $\epsilon s, 3p$), in which the outgoing electron experiences the angular momentum change $\Delta l = \pm 1$ and the excited electron retains its angular momentum, $\Delta l' = 0$, are predominant at photon energies between 130 and 150 eV. Population of the $3p$ state occurs 60 to 80% of the time, which is of a similar magnitude as the 70% population of the analogous $2s$ state of helium[18] at the same relative photon energy. This means that the so-called monopole process $2p^6$-$2p^4\epsilon d, np$ that is predicted in the sudden approximation or shakeoff theory is the most probable process even at relatively low photon energies. As was shown earlier theoretically[41] it would be predominant at photon energies much in excess of the excitation threshold of the shakeoff electron. Several experimental observations are in accord with this prediction: For example, in helium the "monopole" excitation gains in importance with increasing photon energy,[18] and in neon 99% of the $\epsilon l, n'l'$ processes concomitant with K ionization by 1.5-keV photons are "monopole" and only about 1% requires a change of l for the excited electrons, $1s^22s^22p^6 \rightarrow 1s2s^22p^53s, \epsilon s$.[8]

Up to this point we have ignored a process which has a substantial probability in the ionization of argon,[10,42] the configuration interaction $3s3p^6(^2S) \rightarrow 3s^23p^43d(^2S)$ corresponding to $2s2p^6(^2S) \rightarrow 2s^22p^43s(^2S)$ or $2s^22p^43d(^2S)$ in Ne. The latter state occurs at $\Delta E = 38.3$ eV in Fig. 3 and an inspection of the figure shows its contribution to be insignificant, less than 3% of all $\epsilon l, n'l'$ processes. If we were to allot the total $2p^43s$ intensity we just found to amount to less than 25% of peak $7(i)$ to the configuration interaction route, we would find the final state $2s^12p^6$ arising from single s-electron ionization to transform into the state $2s^22p^43s$ in less than 5% of the cases. This estimate should be compared with the theory of Chang *et al.*,[32] who calculate a probability of 2.2% for the related virtual Auger process $2s2p^6 \rightarrow 2s^22p^4\epsilon s$, in which the excited electron goes into a continuum state. The small, if not negligible, probability of the configuration interaction in neon as opposed to that in argon can be understood qualitatively if we consider that in neon interactions take place between different principal shells having a smaller overlap than the subshells of the same principal shell in argon.

As a final observation we note in Fig. 3 the occurrence of peaks that cannot be identified with terms derived from optical-spectroscopy data. We suspect that at least part of them belong to $2p^4nl$, $n \geq 4$, configurations. Few of these states are listed in Moore's Tables.[38] Their total intensity amounts to 36% relative to the intensity of the identified transitions.

As seen from Table IV, peaks $[10(h) + 11(k)]$, $7(i)$, and $3(j)$ can be associated with the states $2p^4(^3P, ^1D,$ and $^1S)$ to which a $3p$ electron has been added. Interestingly enough the theoretical multiplet ratio[43] of 9 : 5 : 1 for these states, which is

observed for example for the magnesium $K\alpha_3$, $K\alpha_4$, and $K\alpha'$ x-ray satellite lines,[44] which have the same final states, is not observed in the present case. Instead a ratio of 9:(17–22):$\lesssim$ 6 is found.

E. Relative intensities of $\epsilon l, n'l'$ transitions in the L shell as a function of photon energy

In Table IV, the relative intensities of $\epsilon l, n'l'$ transitions involving two $2p$ electrons are given for a photon energy of about 140 eV; in this section the intensity variation of peak $7(i)$ with photon energy is reported and discussed. Since we noted that "monopole" transitions are intense even at low energies and should become dominant at higher photon energies [8,18,41] we shall frequently use the term shakeup in the following, implying that the shakeoff theory does provide an adequate description of the $\epsilon l, n'l'$ processes somewhat above threshold.

While the energy dependence of $\epsilon l, \epsilon' l'$ processes, also called shakeoff, has been investigated in several instances,[6,9,12,45] only one qualitative result[11] has been given for the shakeup of KL electrons in neon, and a detailed study has been made of the shakeup process in helium[18] over a wide range of energies. In this experiment we measured probabilities of shakeup involving $2p$ electrons and $2s2p$ electrons of neon over a range of excitation energies from 130 eV to 2 keV. We show in Fig. 6 the intensity of peak $7(i)$ relative to the intensity of the $2p$ photoline as a function of relative excitation energy ϵ/E_0, where $\epsilon = h\nu - E^*$ is the excess energy of the photon $h\nu$ over the energy necessary for the shakeup transition, $E^* = 21.56 + 34.31$ eV for peak $7(i)$, and E_0 is the energy to promote a $2p$ electron in the presence of a $2p$ hole, $E_0 = 34.31$ eV in this case. By adding another ordinate to Fig. 6, giving the relative shakeup intensities for all transitions, see Fig. 3, we express the fact that the intensity of peak $7(i)$ is *approximately* a constant fraction of the total shakeup intensity regardless of energy. Unfortunately, no suitable x-ray lines exist between 300 and 900 eV to be able to unambiguously fix the shape of the curve, but it appears as if a high-energy limit is being reached without going through a maximum. The existence of a maximum has previously been associated[12,46] with the presence of electron-electron correlation and has, in fact, been observed[18] in He, where correlation is strong, and for $\epsilon l, \epsilon' l'$ processes in neon, although in the latter case two contradictory observations[6,12] persist. It is absent, or at least very weak, for shakeup of $2p$ electrons in neon in spite of the correlation in this shell which needs to be invoked to explain the shakeup intensity for $h\nu \to \infty$ and to correctly compute photoionization cross sections.[47] A threshold value of almost 4% is suggested by the data points between 130 and 190 eV. A finite and sometimes large threshold value is characteristic of shakeup processes, whereas a zero value is required for shakeoff events.[48]

Peaks n and o of Fig. 2 are due to shakeup processes involving a $2s$, $2p$ electron pair. In plotting their intensities relative to the intensity of the $2s$ rather than the $2p$ photoline, we take the point of view of the shakeoff theory, which predicts a small probability of shakeup, -off, for an inner electron, e.g., $2s$, when an outer electron, e.g., $2p$, is ionized. Figure 7 shows the energy dependence of the shakeup probability as a function of ϵ/E_0, this time using $E_0 = 39.4$ eV, and $E^* = 48.5 + 39.4$ eV. As for the $2p$ electrons, a finite threshold value and an asymptotic limit are observed, but in contrast to the $2p^6 \to 2p^4 \epsilon l, n'l'$ shakeup, a pronounced maximum occurs at $\epsilon/E_0 \approx 14$. The threshold value

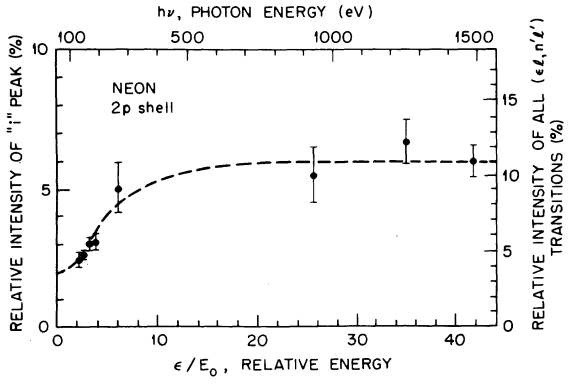

FIG. 6. Energy dependence of the $\epsilon l, n'l'$ process involving two $2p$ electrons and referred to $2p$ photopeak. Points refer to peak $7(i)$ of Fig. 3; right-hand ordinate is auxiliary. Dashed line represents our choice of bridging the gap between 300 and 900 eV.

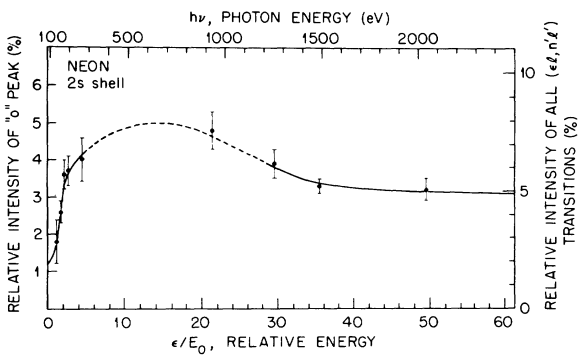

FIG. 7. Energy dependence of the $\epsilon l, n'l'$ process involving a $2s$ and a $2p$ electron and referred to the $2s$ photopeak. Points refer to peak o of Fig. 2; right-hand ordinate is auxiliary.

is about 2% for the shakeup of a $2p$ electron concomitant with the ionization of a $2s$ electron.

Returning to the question whether the shakeup peaks n and o should be associated with the $2s$ photoline and the group comprising peaks 1–12 with the $2p$ photoline we have two comments to add. First, had we referred the n-o group to the $2p$ photoline, we would have obtained a curve starting at a very small threshold value and rising steadily with energy resulting in a shakeup probability of 20% at $h\nu = 2$ keV. In view of previous experience,[9,48] this would be an unlikely behavior both regarding energy dependence and magnitude. Second, had we referred the intensity of peak $7(i)$, representative of the peaks 1–12, to the $2s$ photoline in disregard of the conclusions of Sec. IV D, we would have obtained a curve starting at a high threshold value of about 20% (35% for all transitions) and dropping with energy, giving, for example, a shakeup probability of 2% (4%) at $h\nu = 1.5$ keV. Again, this can be considered improbable, and as a consequence lends a further argument against the assignment of peak $7(i)$ to the configuration-interaction process $2s2p^6(^2S) \rightarrow 2s^22p^4(^2S)3s$.

In Table V, the relative intensities of the shakeup peaks are tabulated. In this table and in Fig. 6, the peak "i" comprises the lines 5–7 plus the faint line 8, since at many x-ray energies these lines could not be resolved. In an earlier paper[7] the strong line o observed with Al $K\alpha$ excitation was suspected to contain some tungsten photolines; however, the smooth alignment of this data point with adjacent points, Fig. 7, removes this suspicion.

TABLE V. Relative intensities of $\epsilon l, n'l'$ transitions (shakeup) involving a $2p^2$ or a $2s2p$ electron pair. Values are given in percent and relative to intensity of parent photoline of single-electron photoionization.

Photon energy (eV)	$2p^2$ Peak $7(i)$	$2p^2$ Total[a]	$2s2p$ Peak n	$2s2p$ Peak o	$2s2p$ Total[b]
132.3	2.49(9)	3.6	...	...	...
151.4	2.61(7)	3.8	1.7(2)	2.6(3)	4.3
171.4	3.0(3)	4.3	...	3.6(4)	...
192.3	3.1(3)	5.2	1.9(3)	3.7(4)	5.6
260.1	5.1(7)	9.0	...	4.0(6)	...
929.7	5.5(1.0)	...	2.1(5)	4.8(5)	6.9
1253.6	6.7(8)	...	2.1(2)	3.9(4)	6.0
1486.6	6.0(5)[c]	11[c]	2.0(2)[d]	3.3(2)[d]	5.3
2042	...	...	1.8(2)	3.2(3)	5.0

[a] Reference $2p$ photoline; $[2p^5(^2P^\circ)]$; $E = 21.565$ eV.
[b] Reference $2s$ photoline; $[2s2p^6(^2S)]$; $E = 48.5$ eV.
[c] According to Carlson *et al.* (Ref. 6).
[d] Carlson *et al.* (Ref. 6) report 1.5 and 2.6% for n and o respectively.

F. Partition of photoionization cross sections

In the preceding sections we have reported cross-section ratios σ_{2s}/σ_{2p} and $\epsilon l, n'l'$ (shakeup) probabilities for ionization in the L shell, but for the partitioning of σ_{tot} into the various constituents, we also need to have $\epsilon l, \epsilon' l'$ (shakeoff) probabilities for ionization in the L shell; and if we exceed the Ne $1s$ threshold, we need additionally ratios σ_{2s}/σ_{1s}, shakeoff and shakeup probabilities for KL electrons. We measured σ_{2s}/σ_{1s} at two energies and found values of 0.040(4) at $h\nu = 1487$ eV and 0.035(3) at $h\nu = 2042$ eV. For shakeoff probabilities concerning only L electrons we used the mean of Carlson's[6] and of Van der Wiel and Wiebes's[12] data, and for the high-energy limit of shakeoff and shakeup probabilities concerning KL electrons we used the evaluation of Krause,[9] namely, $\sigma_s/(\sigma_K + \sigma_s) = 0.14(1) + 0.075(6) = 0.215(10)$, with the first term referring to shakeoff and the second one to shakeup. Correspondingly, we obtain for the L shell $\sigma_s/(\sigma_L - \sigma_s) = 0.12 + 0.07 = 0.19(2)$. The energy dependence of shakeoff of an L electron with K ionization has been investigated recently,[45] and we adopted these results, but for the corresponding shakeup with K ionization we had to assume a shape similar to that given in Fig. 6 in the absence of a specific measurement. (However, besides a value for the high-energy limit, a low-energy point was available and served as a second anchor point.[11]) All data necessary for the partition of σ_{tot} are experimental and could have been obtained solely from measurements employing photoelectron spectrometry had this been the only technique available. However, some data on multiple processes which we have taken from other sources contain also results from Auger-electron and ion spectrometry, techniques especially suited for studying $\epsilon l, \epsilon' l'$ events.

Partitioning of the total photoionization cross section, given by Henke and Elgin[49] and by Wuilleumier,[50] followed the prescription of Eq. (12). Results are plotted in Fig. 8 for $100 \leq h\nu \leq 2000$ eV and are given elsewhere in tabular representation for $50 \leq h\nu \leq 3000$ eV.[20] In that paper, cross sections below 100 eV were extrapolated by following the trend indicated by Kennedy and Manson's calculation.[39] Since then the more sophisticated calculation of Amusia *et al.*[30] has become available, making it necessary to multiply σ_{2s} reported in Ref. 20 by a factor ranging from 0.75 at $h\nu = 50$ eV to 0.95 at $h\nu = 90$ eV. Correspondingly, σ_{2p} should be corrected upward, but

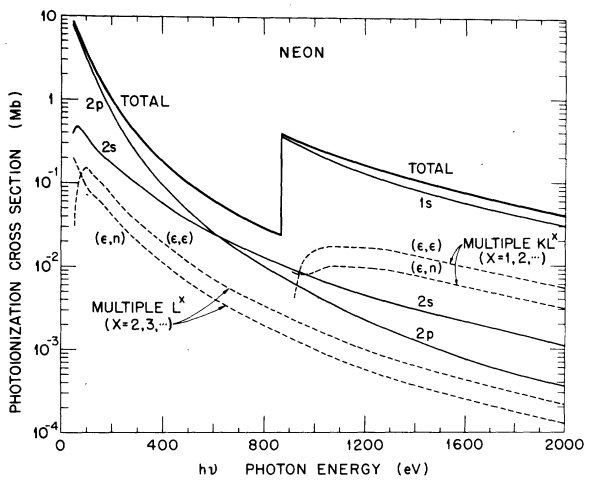

FIG. 8. Partition of total photoionization cross section of neon into its components of single ionization in $2p$, $2s$, and $1s$ subshells, multiple ionization, and simultaneous excitation and ionization in the various subshells. Note that the designations (ϵ,n) and (ϵ,ϵ) omit the quantum number l used in the text.

with $\sigma_{2s}/\sigma_{2p} \lesssim 0.1$, the change is insignificant.

The accuracy of the cross sections for the various processes is estimated from the accuracy of the total and the relative partial cross sections. Based on an accuracy of 2–3% for σ_{tot}, subshell cross sections σ_{nl} are established to an accuracy of better than 10%. A breakdown of our estimates throughout the energy range is given in Table VI.

G. Comparison of subshell cross sections σ_{2p} and σ_{2s} with theory

Identification of all photoionization processes taking place and normalization of measured relative partial cross sections to the absolute total cross section provided us with *absolute* subshell cross sections σ_{2s} and σ_{2p} which can be compared directly with theoretical predictions. However, as pointed out in Sec. III, Eqs. (6) and (7), some caution must be exercised as to the exact meaning of the subshell cross sections *calculated* within different models. In the soft-x-ray region, a number of calculations, some of them extensive, have been carried out in the past ten years, calculations which are based on the central-potential one-electron model introduced by Cooper.[51] The central potential used is the Herman and Skillman (HS) potential and continuum wavefunctions are eigenfunctions of the same potential. Specifically, there are the calculations by Manson and Cooper,[52] who use HS initial and final wave functions; by McGuire,[53] who uses the Cooper model in a slightly different formulation; by Combet-Farnoux,[54] who uses the Cooper model; by Kennedy and Manson,[39] who use Hartree-Fock (HF) continuum wave functions for $h\nu < 400$ eV; and by Scofield,[55] who uses the relativistic version of the Cooper HS model. Disregarding small differences arising from different normalization and numerical procedures, the various calculations give identical results except for the Kennedy and Manson calculation, which in principle at least can be considered superior at low energies because of the use of HF continuum wave functions. In a recent development, Amusia *et al.*[30,47] dropped the independent-particle approximation and incorporated intrashell correlation and intershell interaction through the random-phase method with exchange (RPAE) and the use of HF wave functions. Kelly and coworkers[31] as well as Chang *et al.*[32] have calculated cross sections also for multiple-ionization

TABLE VI. Error estimates (in percent) for photoionization cross section of neon and its constituents in the energy range from 50 to 3000 eV. [Uncertainties of the cross sections for *all* multiple processes are generally smaller than those for the $\epsilon l, n'l'$ and $\epsilon l, \epsilon'l'$ components (see Sec. IV F and Ref. 9).]

Photon energy	Total[a]	$2p$	$2s$	$\epsilon l, n'l'$	$\epsilon l, \epsilon'l'$	$1s$	$\epsilon l, n'l'$	$\epsilon l, \epsilon'l'$
50–100[b]	3	7	12	20	25			
100–200	3	4	6	10	15			
200–870	3	5	7	15	15			
870–1100	2	5	7	15	10	4	30	20
1100–2000	2	7	7	10	10	3	10	10
2000–3000[c]	2	10	8	15	15	3	10	10

[a] According to Henke and Elgin (Ref. 49), below 870 eV, and Wuilleumier (Ref. 50), above 870 eV.

[b] Subshell cross sections σ_{2s} and σ_{2p} extrapolated according to Amusia (Ref. 30). Valid for Fig. 11 and for values of Ref. 20 if corrected according to Sec. IV F. (Corrected values available from authors.)

[c] Extrapolated; see also Ref. 20.

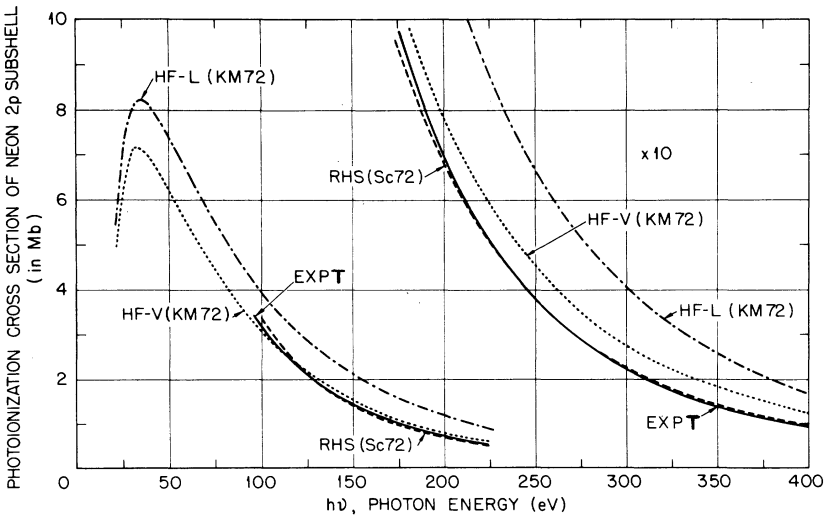

FIG. 9. Experimental subshell cross section σ_{2p} from Fig. 8 compared with theory. HF-*L* and HF-*V*, length and velocity forms of calculation by Kennedy and Manson (Ref. 39). RHS is calculation by Scofield (Ref. 55). Figures 9–11 are drawn carefully to permit scaling; numerical values can be found in Ref. 20. Note that experimental subshell cross sections in Figs. 9–11 refer to *single*-electron transitions.

processes using the Brueckner-Goldstone multibody perturbation theory. From the various calculations, we chose somewhat arbitrarily the calculations of Kennedy and Manson, Manson,[56] and Scofield for comparison with our experimental subshell cross sections σ_{2s} and σ_{2p}, keeping in mind that these calculations are representative of the other calculations of this type. Figures 9–11 show that the simple independent-particle model reproduces σ_{2p} within about 10% over the entire range, if we choose the velocity form of the cross section. Although Scofield's prediction agrees better with experiment, this should not be construed to indicate that relativistic effects are at work at these low photon energies.[57] The surprisingly good agreement between theory and experiment for σ_{2p} is not repeated for σ_{2s}: There the theoretical σ_{2s} lies consistently above the experimental σ_{2s} by 20 to 35%. In contrast to the single-particle model, the model of Amusia *et al.* gives excellent agreement with the experiment in the range where the two sets of data overlap, Fig. 11. This demonstrates the importance and the success of including electron correlation effects in photoionization calculations. These effects though not as dramatic in neon as in argon, krypton, and xenon[4,30,47] are also significant for neon, as this experiment shows. It would be desirable to extend the RPAE calculation to higher energies. Similar good agreement might be expected, since at least for $h\nu \lesssim 1$ keV, no additional processes should come into play and since we excluded in Sec. IV E the possibility of the configuration interaction $2s2p^6 \rightarrow 2s^22p^43s$ draining strength from the single-electron ionization process to any appreciable extent.

The Cooper model, in the calculation of Scofield, overestimates the cross section σ_{1s} to a

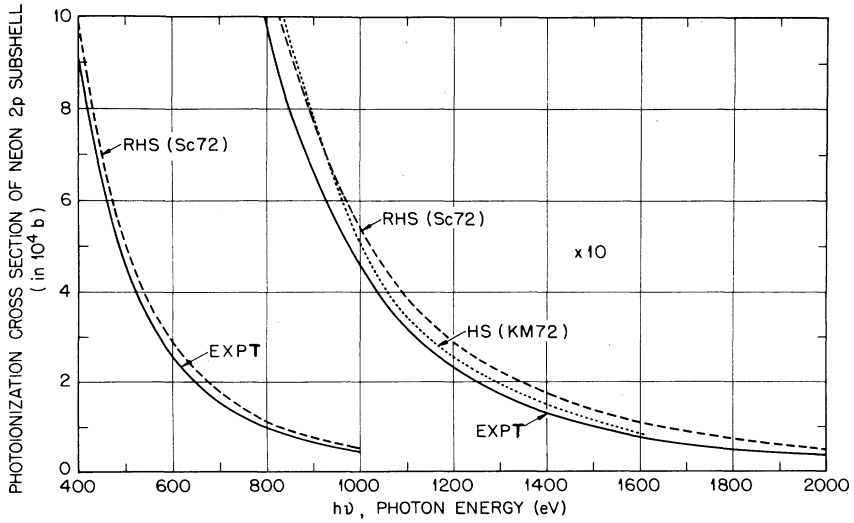

FIG. 10. Subshell cross section σ_{2p}. Extension of Fig. 9 to higher photon energies.

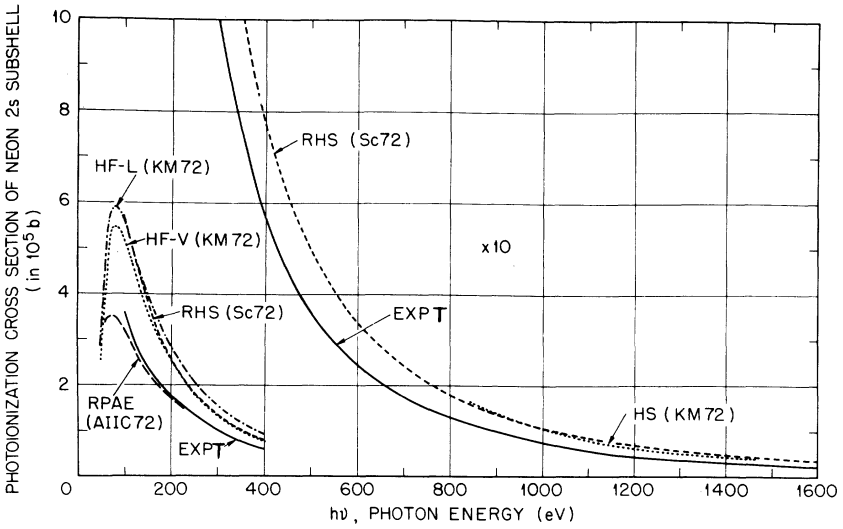

FIG. 11. Experimental subshell cross section σ_{2s} compared with theory. Notations as in Fig. 9, but HS is the calculation by Manson (Ref. 56), and RPAE is the random-phase-approximation-with-exchange calculation by Amusia *et al.* (Ref. 30). The RPAE curve is scaled from Fig. 4 of Ref. 30.

similar degree as the cross sections σ_{2s} and σ_{2p} at energies above 1 keV. At $h\nu = 1.25$ keV, we have $\sigma_{1s,\mathrm{th}} = 1.16\sigma_{1s,\mathrm{expt}}$; $\sigma_{2s,\mathrm{th}} = 1.54\sigma_{2s,\mathrm{expt}}$; and $\sigma_{2p,\mathrm{th}} = 1.29\sigma_{2p,\mathrm{expt}}$. The cross sections for multiple-electron transitions have been calculated only on a relative scale except for one instance, where the multibody perturbation theory was used to calculate $\sigma_{\epsilon l,\epsilon' l'}$ for the L shell at $h\nu = 278$ eV. Chang *et al.*[32] report a value of $(5 \pm 0.2) \times 10^{-20}$ cm^2, which is somewhat larger than the experimental value of $(4 \pm 0.6) \times 10^{-20}$ cm^2. The reason for the mild discrepancy probably lies mostly with the experiment, since the value we selected for normalization is the mean of two different experiments[6,12] that are at variance in this energy region.

V. SUMMARY

Using the technique of photoelectron spectrometry, we have been able to select individual photoionization processes according to the number of electrons ionized or excited, the quantum numbers nl and $n'l'$ of initial and final states, and the angular distributions of the ejected photoelectrons. We identified the processes that take place and measured their relative cross sections in the energy range from 100 eV to 2 keV, in which range the photoabsorption cross section is equivalent to the photoionization cross section since photon scattering processes play a subordinate role. With the data at hand, we could divide the total photoionization cross section, which has been established reliably in many experiments by a number of workers, into its components on a purely experimental basis without the need of invoking theory, thus allowing a more rigorous and detailed test of theory than is provided by a comparison of the total cross sections only. Specifically, we checked the theoretical predictions of $2p$, $2s$, and $1s$ subshell cross sections against our experimental subshell cross sections and find the central-potential independent-particle model, which in general uses Herman-Skillman wave functions, to reproduce the gross features satisfactorily over the entire energy range, but inadequately if we require an accuracy of better than 10%, which is a very modest accuracy if we have to depend on theoretical predictions in other energy ranges and for other elements where no experimental determinations exist. The agreement between experimental and theoretical subshell cross sections is, however, much improved if we interpret the cross sections obtained in the Cooper-Herman-Skillman model as containing both single- and multiple-photoionization processes. In fact, a very recent analysis of the problem has shown[29] that this is the correct interpretation whenever the frozen-structure approximation is employed as in the customary photoionization calculations.

On the other hand, the Hartree-Fock RPAE calculations of Amusia and co-workers[30] agree excellently, that is, within the error limits of about 5%, with our data on the neon $2s$ subshell cross section. Although the calculations have not been carried out over the entire range of this experiment, the present test and a test involving the $3s$ subshell cross section of argon near threshold[4] suggest that calculations of this type should prove dependable in predicting subshell cross sections over an extended range of energies and elements.

Although multiple-photoionization processes have been known for a long time, originally by

way of the x-ray satellites, their occurrence has been largely ignored in photoionization cross-section calculations, not too surprisingly, since up until recently choice of the potential and wave functions resulted in a much greater effect than multiple processes. As theoretical predictions for single-electron photoionization are becoming more dependable, multiple processes are gaining in importance from the theoretical point of view. In this experiment we have reported absolute cross sections for multiple processes in the various subshells. There exists a single theoretical value that can be compared with experiment: the experimental cross section for double ionization in the L shell of neon, which has a value of 4×10^{-20} cm^2 at $h\nu = 278$ eV, which compares favorably with the theoretical value of 5×10^{-20} cm^2.

Simultaneous excitation and ionization processes in the L shell have been investigated in detail, demonstrating that shakeup processes, in which the ionized electron changes the angular momentum l but not the excited electron, are strong even at low energies, $h\nu \approx 150$ eV. Configuration-interaction processes that lead to an excited ionic state, found to be strong in argon, are found to be weak, if not absent, in neon.

ACKNOWLEDGMENTS

It is a pleasure to acknowledge the generous help of Dr. S. T. Manson, Atlanta, Dr. J. Scofield, Livermore, and Dr. F. Combet-Farnoux, Paris, who all supplied, and allowed the use of, data prior to publication, and of Dr. J. Cooper, NBS, and Dr. T. Åberg, Helsinki, who made constructive comments.

---

*Research sponsored by the U. S. Atomic Energy Commission under contract with the Union Carbide Corp.

†Present address: Laboratoire de Chimie Physique, Bât 350, and Laboratoire pour l'Utilisation du Rayonnement Electromagnetique émis par l'Anneau de Collisions d'Orsay, Université Paris-Sud, 91405 Orsay, France.

[1]M. O. Krause, Phys. Rev. 177, 151 (1969).

[2]J. A. R. Samson and R. B. Cairns, Phys. Rev. 173, 80 (1968).

[3]K. Siegbahn, C. Nordling, G. Johansson, J. Hedman, P. F. Heden, K. Hamrin, U. Gelius, T. Bergmark, L. O. Werme, R. Manne, and Y. Baer, *ESCA Applied to Free Molecules* (North-Holland, Amsterdam, 1969).

[4]M. J. Lynch, A. B. Gardner, K. Codling, and G. V. Marr, Phys. Lett. A 43, 237 (1973).

[5]M. O. Krause, T. A. Carlson, and R. D. Dismukes, Phys. Rev. 170, 37 (1968).

[6]T. A. Carlson, Phys. Rev. 156, 142 (1967).

[7]T. A. Carlson, M. O. Krause, and W. E. Moddeman, J. Phys. (Paris) 32, C4-76 (1971).

[8]U. Gelius, E. Basilier, S. Svensson, T. Bergmark, and K. Siegbahn, J. Electron Spectr. 2, 405 (1973).

[9]See the brief reviews: M. O. Krause, J. Phys. (Paris) 32, C4-67 (1971); and M. O. Krause, in *Inner Shell Ionization Phenomena and Future Applications*, edited by R. W. Fink, S. T. Manson, J. M. Palms, and P. V. Rao, U. S. AEC Conference-72-0404 (Natl. Tech. Info. Service, U. S. Dept. of Commerce, Springfield, Va., 1973), p. 1586.

[10]D. P. Spears, H. J. Fischbeck and T. A. Carlson, Phys. Rev. A 9, 1603 (1974).

[11]M. O. Krause, T. A. Carlson, and W. E. Moddeman, J. Phys. (Paris) 32, C4-139 (1971).

[12]M. J. Van der Wiel and G. Wiebes, Physica 54, 411 (1971).

[13]G. S. Lightner, R. S. Van Brunt, and W. D. Whitehead, Phys. Rev. A 4, 602 (1971).

[14]T. A. Carlson and A. E. Jonas, J. Chem. Phys. 55, 4913 (1971), and references cited therein.

[15]A. Niehaus and M. W. Ruf, Z. Phys. 252, 84 (1972).

[16]M. J. Van der Wiel and C. E. Brion, J. Electron Spectr. 1, 439 (1972/73).

[17]M. J. Lynch, A.B. Gardner, and K. Codling, Phys. Lett. A 40, 349 (1972).

[18]M. O. Krause and F. Wuilleumier, J. Phys. B 5, L143 (1972); F. Wuilleumier and M. O. Krause (unpublished).

[19]F. Wuilleumier and M. O. Krause, in *Electron Spectroscopy*, edited by D. A. Shirley (North-Holland, Amsterdam, 1972), p. 259.

[20]F. Wuilleumier, Adv. X-Ray Anal. 16, 63 (1973).

[21]M. O. Krause, Adv. X-Ray Anal. 16, 74 (1973).

[22]M. O. Krause, Chem. Phys. Lett. 10, 65 (1971), and references therein.

[23]K. Siegbahn, C. Nordling, A. Fahlman, R. Nordberg, K. Hamrin, J. Hedman, G. Johansson, T. Bergmark, S. E. Karlsson, I. Lindgren, and B. Lindberg, *ESCA, Atomic, Molecular and Solid State Structure Studied by Means of Electron Spectrometry* (Almquist and Wiksells, Uppsala, 1967).

[24]R. Kollath, Ann. Phys. 27, 721 (1936).

[25]M. O. Krause, Phys. Lett. 19, 14 (1965).

[26]The simple reduction by $\sin\theta$ was used, introducing an error not greater than 1%. [P. J. Volz, thesis (University of Nebraska, 1968) (unpublished).]

[27]For high-Z elements $\beta_{n0} < 2$, however. [T. E. H. Walker and J. T. Waber, Phys. Rev. Lett. 30, 307 (1973); and Ref. 15].

[28]J. W. Cooper and S. T. Manson, Phys. Rev. 177, 157 (1969).

[29]C. S. Fadley, Chem. Phys. Lett. 25, 225 (1974).

[30]M. Ya Amusia, V. K. Ivanov, N. A. Cherepkov, and L. V. Chernysheva, Phys. Lett. A 40, 361 (1972).

[31]H. P. Kelly, Phys. Rev. A 6, 1048 (1972).

[32]T. N. Chang, T. Ishihara, and R. T. Poe, Phys. Rev. Lett. 27, 838 (1971).

[33]Relative intensities of double-ionization processes were not remeasured but taken from earlier work, as described in Ref. 9.

[34]S. Goudsmit and L. Gropper, Phys. Rev. 38, 225 (1931).

[35]K. Codling, R. P. Madden, and D. L. Ederer, Phys. Rev. 155, 26 (1967).
[36]M. Peshkin, Adv. Chem. Phys. 18, 1 (1970).
[37]S. T. Manson, J. Electron Spectr. 7, 413 (1972/73).
[38]C. E. Moore, *Atomic Energy Levels*, NBS Circular 467 (U. S. GPO, Washington, D. C., 1949), Vol. 1.
[39]D. S. Kennedy and S. T. Manson, Phys. Rev. A 5, 227 (1972).
[40]This should not be construed to mean that all peaks have p character since those with d character might have a similar dependence, for probably $\beta_d \approx \beta_p$ in contrast to $\beta_p < \beta_s$. A high-precision measurement would be necessary to discern possible small differences in the angular distribution.
[41]E. E. Salpeter and M. H. Zaidi, Phys. Rev. 125, 248 (1962).
[42]J. W. Cooper and R. E. LaVilla, Phys. Rev. Lett. 25, 1745 (1970).
[43]E. H. Kennard and E. Ramberg, Phys. Rev. 46, 1040 (1934).
[44]M. O. Krause and J. Gomes Ferreira (unpublished).
[45]T. A. Carlson, W. E. Moddeman, and M. O. Krause, Phys. Rev. A 1, 1406 (1970).
[46]F. W. Byron and C. J. Joachian, Phys. Rev. 164, 1 (1967).
[47]M. Ya. Amusia, N. A. Cherepkov, and L. V. Chernysheva, Zh. Eksp. Teor. Fiz. 60, 160 (1971) [Sov. Phys.—JETP 33, 90 (1971)].
[48]T. Åberg, in Ref. 9, p. 1509. This review cites further work, especially on theoretical aspects.
Manson, J. M. Palms, and P. V. Rao, U. S. AEC Conference-72-0404 (U. S. GPO, Washington, D. C., 1973), p. 1509. This review cites further work, especially on theoretical aspects.
[49]B. L. Henke and R. L. Elgin, Adv. X-Ray Anal. 13, 639 (1970).
[50]F. Wuilleumier, Compt. Rend. B 270, 272 (1970); J. Phys. (Paris) 26, 776 (1965).
[51]J. W. Cooper, Phys. Rev. 128, 681 (1962).
[52]S. T. Manson and J. W. Cooper, Phys. Rev. 165, 126 (1968).
[53]E. J. McGuire, Phys. Rev. 161, 51 (1967).
[54]F. Combet-Farnoux, J. Phys. (Paris) 30, 521 (1969).
[55]J. Scofied, Lawrence Livermore Laboratory, Report No. UCRL 51326, 1973 (unpublished), and private communication.
[56]S. T. Manson (private communication).
[57]For example, the recent nonrelativistic calculation of F. Combet-Farnoux and M. Lamoureux (private communication) by this model (Refs. 51 and 54) agrees excellently with Scofield's calculation.